Erosion Resistance of Tungsten-Carbide Coatings for Steel Pipes in Fluid Catalytic Cracking Units

Group Members:
Jennifer Hulfachor
Davis Vannasing

Advisor:
Dr. Trevor Harding

Sponsor:
Chevron ETC – Richmond California
Jessica Williams
Maricela Johnson

MATERIALS ENGINEERING
California Polytechnic State University

June 11th, 2019

1. Abstract

In petroleum processing, the flow of catalyst readily leads to erosion of piping in a fluid catalytic cracking unit. Advances in coating materials and processes necessitate a re-evaluation of current protection methods. Commercially available tungsten-carbide (WC) claddings and nanostructured WC-W CVD coatings were investigated as potential alternative erosion-resistant coatings. Erosion tests by solid particle impingement were conducted on 2 variations of claddings and 1 variation of WC-W coatings following ASTM standard G76. A36 steel coupons were used as reference samples. For statistical validation, 2-3 replications of the tests were performed for the claddings and WC-W coating. Testing was conducted using a sandblasting apparatus with 70 μm alumina powder at an impingement angle of 90° and 25°. Data obtained for each cladding, as well as A36 steel, was used to plot mass loss versus time, resulting in erosion rates. Average erosion values were reported as volume loss per gram of abrasive with units of mm^3/g. The claddings displayed similar erosion values at 90°, but both were less resistant than bare A36 steel. Optical and electron microscopy of the cladding interface revealed coherent bonding across the interface and no obvious voids in the coating or at the interface. The microstructure of the steel substrate consisted of large regions of pearlite embedded in a ferrite matrix; therefore, improper heat treatment cannot be used to explain the superior erosion resistance. At 25°, the WC-W coating and claddings performed similarly and both resisted erosion better than A36 steel.

2. Introduction

2.1 Stakeholders

The results of our experiment regarding erosion resistant coatings has the potential to benefit or disbenefit a variety of stakeholders including:

- Cal Poly senior project students
- Chevron ETC
- Chevron Corporation
- Other oil companies using FCC
- Oil consumers
- Suppliers of Stellite
- Suppliers of erosion resistant coatings
- Consumers requiring erosion resistant coatings
- Corrosion engineering community

We, as the students undertaking this senior project, can benefit if our research successfully provides insight into the nature of these coatings, thereby, reflecting well on our ability to solve problems and present solutions leading to our increased knowledge and credibility. Chevron ETC can benefit if our findings lead to the selection of an alternative coating that meets most or all of their requirements. This would lead to cost savings for Chevron ETC and Chevron corporation as a whole. This could also increase the safety of the operation if the coating is more effective at preventing corrosion, so there is less risk of pipe failure. If the project yields no usable information, then Chevron will have invested time and money into an issue that remains unresolved. Other oil companies using FCC could also benefit from improved erosion resistant coatings for their operations. If the efficiency of oil processing is increased, it may lead to savings for consumers of refined oil products, such as drivers of vehicles. If testing shows greater benefits for alternative erosion resistant coatings, this could mean increased business for the suppliers of these products and a reduction in business for suppliers of Stellite. Consumers who require erosion resistant coatings could benefit if further information is available about alternative coatings that could save them money. Corrosion engineers could better service clients' erosion problems by recommending the best possible solution for their needs.

2.2 Broader Impacts

2.2.A - Benefits

The benefits that could arise from the results in this project involve improvements to the fluid catalytic cracking operation including cost reduction, increased longevity of the unit, and safe continuous operation. Cost reduction could be possible if the alternative coating to the current Stellite costs less to purchase, can be applied in a thinner coat, and can be more easily applied to large or small diameter piping. If the new coating has improved adhesion to steel pipes and is able to form a hard, dense layer while offering resistance to corrosion such as sulfidation, then the FCC unit could operate longer without needing costly maintenance as frequently. Prevention of corrosion allows the pipes to continue to be in operation without diminished mechanical properties, which reduces the chance of leaks or failure over time. An improved FCC process could have economic benefits for suppliers and consumers of oil, and these benefits could extend to various other applications that suffer from erosion.

2.2.B - Risks

It is possible that this project may not yield any useful information leading to the selection of a superior coating to Stellite, either because of an invalid experiment or because no superior coating was found or exists yet. This would mean that Chevron invested their time and money into a fruitless endeavor, and the Cal Poly students working on the project would lose some credibility. If an alternative coating were to be selected and eventually used to replace Stellite, it would be possible that this coating could fail in an unpredicted manner. This could lead to high speed, high temperature, hard particles rupturing from the pipes causing harm to humans, equipment, or the environment. On a less extreme note, it may only cost extra to replace corroded pipe if the alternative coating proves ineffective over time.

2.2. C - Ethics

It may frequently be a temptation to sacrifice production quality and safety for cost reduction. The safety of other people and protecting the environment should be the top priority. It may also be a temptation to falsify data in order to make it appear that an experiment was successful and provided invaluable information thanks to the aspiring ingenuity of those who designed and conducted it. It is of the utmost importance to be as accurate as possible regarding experimental findings as well as to articulate the degree of validity for all aspects of the project. Further, any proprietary information divulged to senior project students by the sponsor should be held in confidence and in accordance with what is agreed upon.

3. Background

3.1 Petroleum Processing

3.1.A - Chevron Corporation

Chevron, a successor company of Standard Oil, is a multinational energy corporation, engaged in every aspect of the oil, natural gas, and geothermal energy industries (Wikipedia 2019). The latter including hydrocarbon exploration and production, refining, chemical manufacturing, and power generation. Chevron manufactures and provides products such as fuels, lubricants, additives, and petrochemicals.

3.1.B - Petroleum Properties

Petroleum is a key substance that propels modern society. It provides fuel and energy for transportation, and is also used in polymers, paints, fertilizer, and medicine. The composition of petroleum varies depending on deposit location, but the percentage of chemical elements changes over fairly narrow limits (Ancheyta 2011). Carbon and hydrogen account for a majority of the composition (Table I). Sulfur, nitrogen, oxygen, and metals are present in relatively low quantities. Crude oil (petroleum) resides deep underground where residue of plants and animals have been heated up and pressurized over millions of years. Crude oil is a blackish viscous liquid and gives off a sulfur odor (Figure 1) (AAPG).

Table I: Typical Elemental Composition of Petroleum

Element	Weight Percentage
Carbon	84-87
Hydrogen	11-14
Oxygen	0.1-0.5
Nitrogen	0.1-2
Sulfur	0.5-6
Metals	0-0.1

Figure 1: Physical characteristics of raw petroleum oil.

3.1.C - Fluid Catalytic Cracking (FCC)

The fluid catalytic cracking process is the core of modern refinery, intended to maximize gasoline production from crude oil feed. As a result of higher gasoline yields, the FCC process provides the greatest potential for increasing profitability within the entire refining process (Ancheyta 2011). The process increases hydrogen/carbon ratio by hydrogen rejection in a continuous process, converting the high temperature and high molecular weight hydrocarbon fraction into a more valuable product.

The two main components of an FCC system consist of an interconnected reactor and regenerator. This configuration allows for transferring consumed catalyst from the reactor to the regenerator, and the regenerated catalyst from the regenerator to the reactor (Ancheyta 2011). During the process of catalytic cracking, the feed is vaporized and the long-chain molecules are cracked into much shorter molecules by physical contact with the feed and fluidized powdered catalyst at about 535 ˚C and 25 psi (Wikipedia 2019).

The following carbonium ion mechanism pertains to catalytic cracking, involving the following steps:

1. Initiation: starts with early contact of an olefin with an active catalyst site at high temperature to produce the active complex corresponding to carbocation formation.
2. Propagation: transfer of hydride ion from a reactant molecule to an adsorbed carbenium ion.
3. Termination: corresponding to the desorption of the adsorbed carbenium ion to produce an olefin while initial active catalyst site is restored.

Through this mechanism, a catalyst promotes the removal of a negatively charged hydride ion from a paraffin compound, or the addition of a positively charged proton (H^+) to an olefin compound. The latter results in the formation of a carbonium ion, which is a positively charged molecule that acts as an intermediate compound to transfer the charge through the hydrocarbon. This transfer continues as the hydrocarbon compounds contact the active sites on the hydride ions surface. This weakens the covalent carbon - carbon bonds of the hydrocarbon molecules, consequently cracking into smaller components.

Coke formation is inevitable in the catalytic cracking process due to dehydrogenation and condensation of polyaromatics and olefin (Ancheyta 2011). Rapid deactivation caused by blocking active catalyst pores is a consequence of coke deposition. While these reactions occur, the cracked gasoline produced retains large amounts of aromatics and branched compounds, which is advantageous for the gasoline's octane content.

A modern FCC unit consists of the following steps (Figure 2):

1. Preheating the feed, then mixing with recycled slurry from the bottom of the distillation column.
2. Injecting the combination above into the catalyst riser to vaporize.

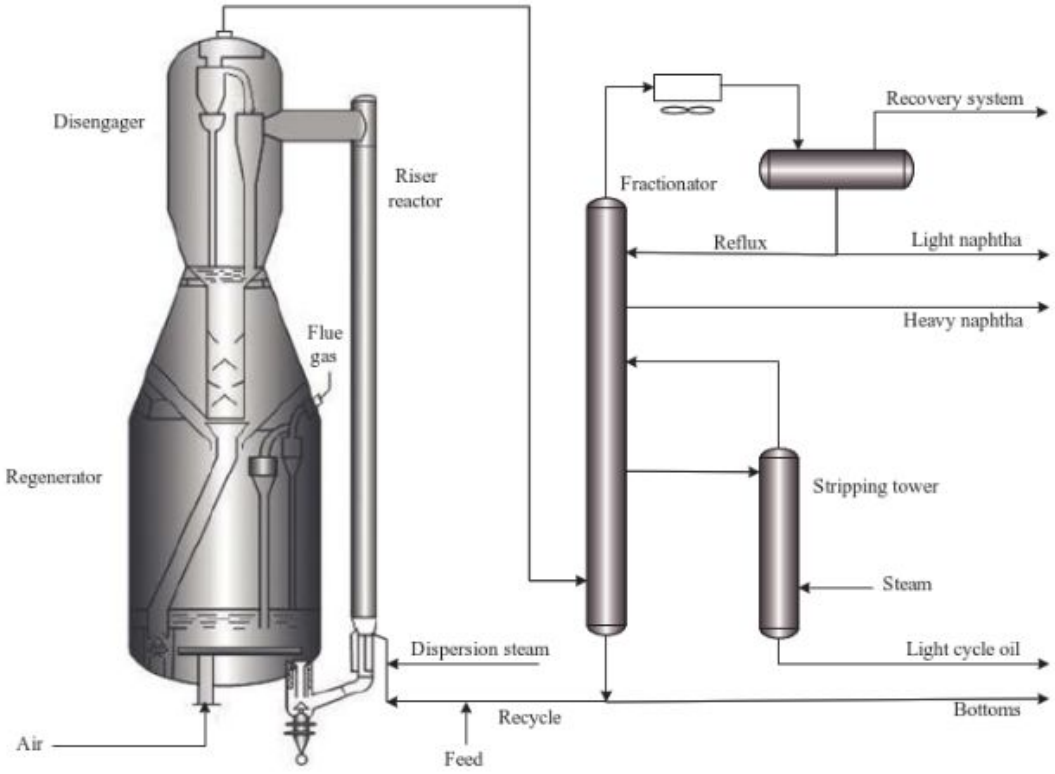

Figure 2: A typical modern fluid catalytic cracking process flow diagram, displaying feed and recovery of pre-distilled vacuum gas oil (VGO), heavy gas oil (HGO), or residue feedstocks in conjunction with catalyst.

3.1.D - Catalyst Characteristics

An FCC catalyst must fulfill a variety of requirements including the ability to selectively convert large feedstock molecules into desired products, withstand impacts with other catalyst molecules and pipe walls during circulation, withstand high temperatures and pressures, withstand interactions with poisons and metals in heavier feedstock, produce the minimum amount of coke, and retain the ability to fluidize. These requirements are achieved through the formation of a complex spherical particle, approximately 70 μm in diameter, composed of zeolite, alumina, silica, and clay (Figure 3). Zeolite is the main active component composed of tetrahedrally linked silicate with aluminum in some of the silicon lattice positions. The porous structures in the zeolite capture larger molecules and the acid sites allow conversion into smaller gasoline molecules. Alumina and silica act to bind the catalyst together and offer a macroporous structure with acid sites to pre-crack the largest molecules from the feedstock before conversion in the zeolite. Clay is a filler that also helps with heat capacity. Over the course of about a

month, the catalyst will deactivate as it is steamed during regeneration and impregnated with metals such as nickel (Ni) and vanadium (V). To account for deactivation, fresh catalyst is periodically exchanged with an equal amount of the bulk catalyst in the regenerator (Vogt 2015).

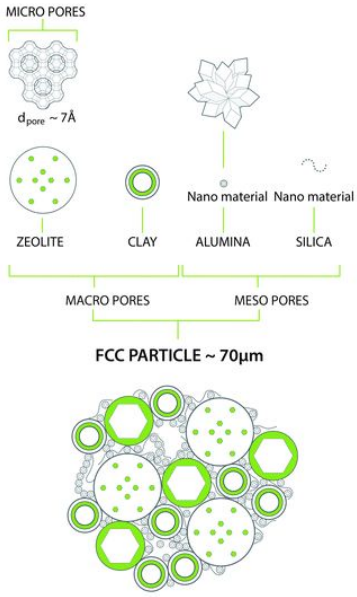

Figure 3: Representation of an FCC catalyst structure.

3.1.E - Erosion due to Flow of Catalyst

The continuous flow of catalyst through the FCC unit at temperatures and speeds up to 760 °C and 40 m/s, respectively, eventually leads to extensive internal erosion of the piping. The equipment walls and internals are at risk of experiencing material loss as the catalyst particles impact surfaces at various angles. This form of erosion is known as solid particle impingement erosion. Sections where catalyst velocity rises, such as the riser outlet and the inlet to the primary cyclones in the reactor and regenerator, can experience the highest erosion rates. Erosion within the FCC unit can directly limit the continuous run-life of the unit to about 5 years before internal components must be repaired or replaced (Murphy 1994).

3.2 Evaluation of Erosion in FCC Units

3.2.A - Solid Particle Erosion

The form of corrosion categorized as erosion-corrosion is a combination of both chemical and mechanical corrosive attack, with mechanical wear causing accelerated deterioration. Although erosion-corrosion may contribute to failure in FCC pipes, the mechanical aspect of erosion due to flow of catalyst is the focus of this investigation. FCC unit deterioration is primarily caused by solid particle

impingement from the catalyst which is fluidized using gas jets. Solid particle erosion (SPE) is the loss of material resulting from repeated impact of solid particles suspended in a carrier fluid. Carrier fluids range from gas, liquid, steam, and multiphase flow. SPE is expected when hard particles suspended in a fluid medium impinge on a solid at velocities greater than 1.0 m/s (Wood 2017). At catalyst speeds up to 40 m/s, it can be assumed that SPE is occurring.

3.2.B - Factors Influencing Erosion

There are several variables that impact the severity of erosion which can be separated into 3 categories: impingement variables, particle variables, and material variables. The geometry and composition of the eroding material in conjunction with the properties and parameters of the flowing particles can result in dramatically different outcomes. Impingement variables include particle velocity, angle of incidence, particle concentration, particle mass, particle size, and carrier fluid viscosity. Depending on whether the material is brittle or ductile, the angle of impingement has different effects on erosion rate. Turbulent flow of particles as well as bends in piping can lead to 90° impacts that can be more detrimental to brittle materials. Sliding wear, or abrasion, at more oblique angles can be more detrimental to ductile materials. Additional particle variables include particle shape, hardness, kinetic energy, flux, and ease of fracture. Important properties to consider for erosion resistant materials include hardness, fracture toughness, operating temperature, residual stress, surface treatment, and microstructural flaws. Due to the sensitivity of erosion behavior to a variety of properties, ranking erosion resistance is difficult, and comparisons can only be made under highly controlled testing conditions (Wood 2017).

3.2.C - Erosion Control

There are five methods used to prevent or minimize corrosion (Davis 2000):

1. Coatings - are arguably the most common corrosion control method. Protective coatings are divided into metallic and nonmetallic. Metallic coatings are often applied as noble metal protection or sacrificial anode protection against galvanic corrosion; an example being a sacrificial zinc coating on galvanized steel. Nonmetallic coatings are either organic or inorganic. Organic coatings, or paint, primarily function as a barrier to corrosive environments. An example of an organic coating is solvent-based acrylic used as an automotive finish. Inorganic coatings include hard ceramic coatings that possess wear-resistant and heat-resistant protective capabilities.

2. Cathodic Protection - systems are designed to reduce chemical erosion by redirecting current flow, produced from an electrochemical corrosion cell, toward the material to be protected. This means metal loss will not occur at the protected metal surface due to ion formation. This is accomplished using either sacrificial anodes or impressed current systems. In order for cathodic protection systems to be effective, an electrolyte must be present, which completes the corrosion cell. Because it is assumed that catalyst flow occurs in dry gas jets, cathodic protection systems would not be a useful solution.

3. Materials Selection - Proper materials selection involves understanding the specific erosive conditions. For high temperature applications and high impingement velocities, a material must be selected that possesses sufficient high temperature strength and toughness. All material variables, previously listed, that influence erosion must be considered in conjunction with particle properties.

4. Inhibitors - are chemical species that can inhibit corrosion depending on the material and environment. Inhibitors are best used in closed systems and can be added to coatings or primers. This investigation does not focus on the chemical impacts of corrosion and, therefore, will not go into detail about the use of inhibitors.

5. Design - recommendations include optimizing pipe diameter to encourage lamellar flow and proper fluidization, changing the diameter of streamline bends to optimize impingement angles, increasing material thickness in vulnerable areas, avoiding excessive increases in velocity due to narrow inlets/outlets, designing susceptible equipment to be easily replaceable, and extending 90° bends to form a T-section that can capture incoming abrasive which can eventually form a protective layer.

Application of wear resistant coatings to a substrate material is one of the most common erosion control methods. Tribology, or the study of wear, friction, and lubrication, is applied to various coatings engineered for the purpose of erosion protection (Cotell 1994). The application of coatings for mechanical erosion protection will be the primary method considered for this research, which will also lead to design recommendations.

3.3 Desirable Properties of Internal Erosion-Resistant Coatings

3.3.A - Hardness and Fracture Toughness

Abrasive wear occurs when the abrading material contacts a surface of lower hardness. This results in scratching, indentation, fracture, and volume loss of the eroding material. It can, therefore, be beneficial to increase the hardness of surfaces at risk of erosion. Some high hardness coatings include hard alloys, which contain large amounts of hard phases that form during solidification, and metal-matrix composites (MMC), which consist of a metal (usually cobalt, nickel, or iron) matrix dispersed with hard ceramic particles (Theisen 2017). Plotting hardness against abrasive wear resistance, measured using ASTM standards, it is apparent that there is a positive correlation (Figure 4).

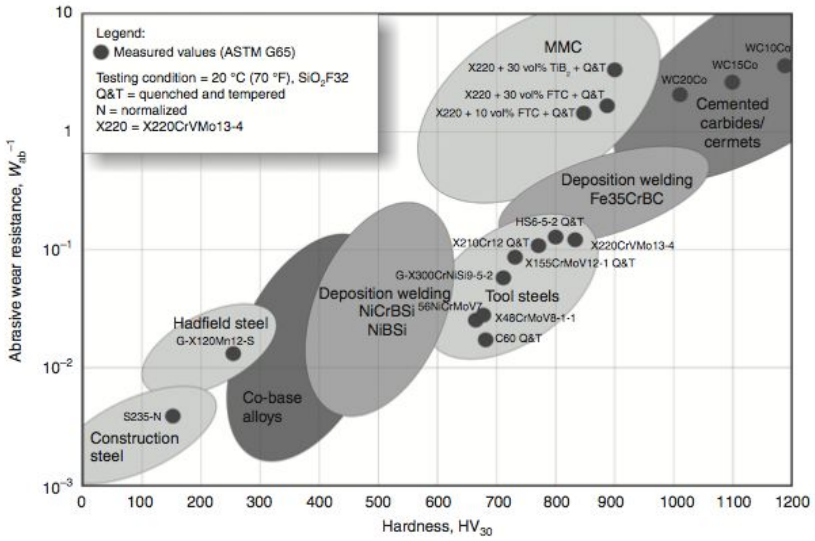

Figure 4: Relationship between three-body abrasion wear resistance and Vickers hardness of various materials designed for erosion resistance.

The ability of a coating to resist crack propagation due to the impacts from abrasive particles is also an important property, quantitatively measured by fracture toughness. The combination of hardness and fracture toughness results in different erosion micromechanisms (Figure 5). As hardness increases and fracture toughness decreases, erosion failures become more characteristic of brittle materials rather than ductile materials (Theisen 2017). The mechanisms of ductile erosion include cutting and deformation. Cutting occurs at lower angles of impingement and results in material loss through what can be thought of as chip formation. Deformation occurs more at near 90° impingement angles and results in plastic deformation of the surface. Ductile erosion increases with abrasive particle size until about 50 - 100 μm, at which point the erosion rate levels off.

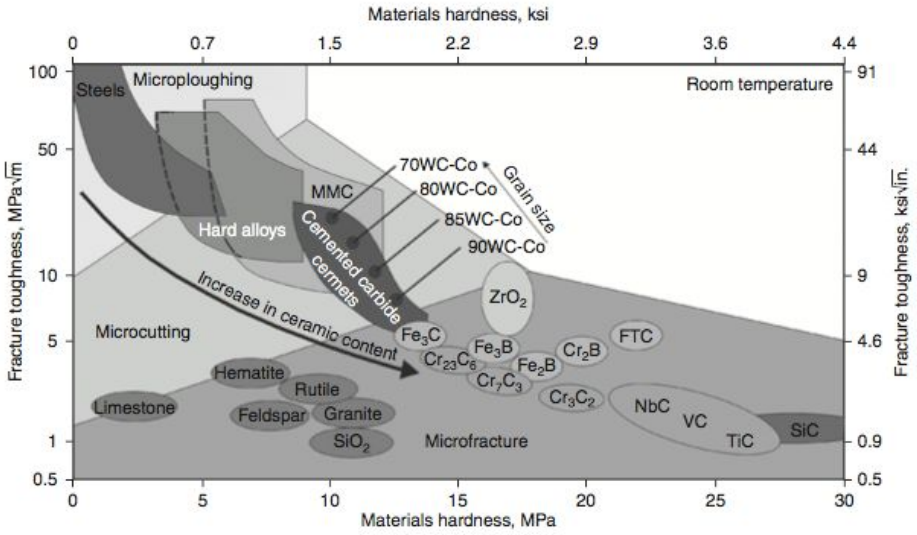

Figure 5: Wear micromechanisms of various materials with different hardness and fracture toughness values.

There is a similar trend with particle hardness where the erosion rate increases as the hardness of the impacting particle increases relative to the impacted surface then levels off at a certain point. Solid particle erosion failure in brittle materials occurs due to brittle fracture where crack propagation occurs, leading to material mass loss. Erosion rate in brittle materials has been correlated with the shape, velocity, and mass of the impacting particle. More oblique angles of impingement tend to cause much higher erosion rates in ductile materials than in brittle materials (Figure 6). 90° impingement is a severe form of erosion sometimes called impingement attack than can occur in sharp elbows, leading to deep pits (Adler 2002). Hard, brittle coatings typically perform better under sliding erosion and tend to fail spontaneously under impact loadings (Theisen 2017).

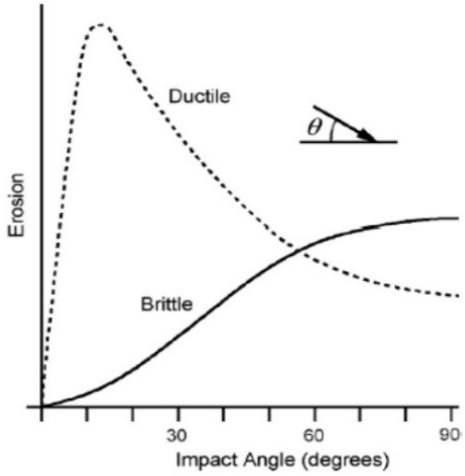

Figure 6: Plot of trends in severity of erosion for ductile and brittle materials based on the angle of impingement of erosive media (Lee 2013).

3.3.B - Adhesion

It is necessary for a coating to adhere well to the substrate in order to maximize mechanical properties and minimize delamination. Impurities and vacancies can interfere with proper adhesion and lead to porosity in the coating. In metal-to-metal interfacing, large impurities such as bismuth, sulfur, and phosphorous, lower grain boundary adhesion. Scanning electron microscopy (SEM) and metallography can be used to characterize the interface between the coating and substrate. This can help determine the continuity of the interface, the porosity of the coating, and any diffusion or cross-over grains. Secondary electron SEM can show topological differences at the interface while backscatter electrons can show phase differences. Metallography can also show distinct phases and grain boundaries at lower magnification. Among the most promising characterization techniques for studying interfaces is scanning tunneling microscopy (STM) which can measure electronic behavior as well as the grain boundaries of dissimilar metal interfaces (Dixon 2009).

3.3.C - Ease of Application

The application method directly affects the quality of adhesion and can be a determining factor for how intricate coated surfaces can be to achieve an even application. There are several application methods for hard alloys and ceramic coatings which have excellent high temperature wear resistance properties. Some of these methods include welding deposition, thermal spraying, cladding by sintering, and chemical vapor deposition (CVD). Deposition welding and cladding result in thicker coating layers than thermal spraying while CVD provides thin-film coatings. CVD can be of benefit due to its ability to deposit material on intricate surfaces (Theisen 2017). Common organic coatings such as polyurethanes and epoxies tend to have lower hardness values compared to ceramics and hard metal alloys as well as lower operating temperatures so are usually not the most suitable for more severe environments. Currently, Chevron manages erosion of FCC pipes by applying Stellite, a type of erosion resistant coating.

3.4 Characteristics and Properties of Stellite

3.4.A - Coating Composition

The wear resistant coating currently used by Chevron, Stellite, was produced by Kennametal and has been widely used and tested to perform under highly erosive conditions. Stellite alloys are mostly cobalt-based with various additions of chromium, carbon, tungsten, and/or molybdenum. These alloys have demonstrated resistance to cavitation, corrosion, erosion, abrasion, and galling. Stellite 6 is the most

versatile of the alloys, offering a balance of desirable properties. For a more detailed breakdown of Stellite alloys, see appendix A (Kennametal).

The presence of carbon aids in the formation of hard phases during solidification by precipitating with hard-phase forming elements such as chromium and molybdenum. Micrographs of Stellite 6 show hard phases dispersed in cobalt in the as-cast condition, offering resistance to scratching and deformation. Further HIP processing can form more finely dispersed spherical hard phases that can improve fracture toughness (Figure 7).

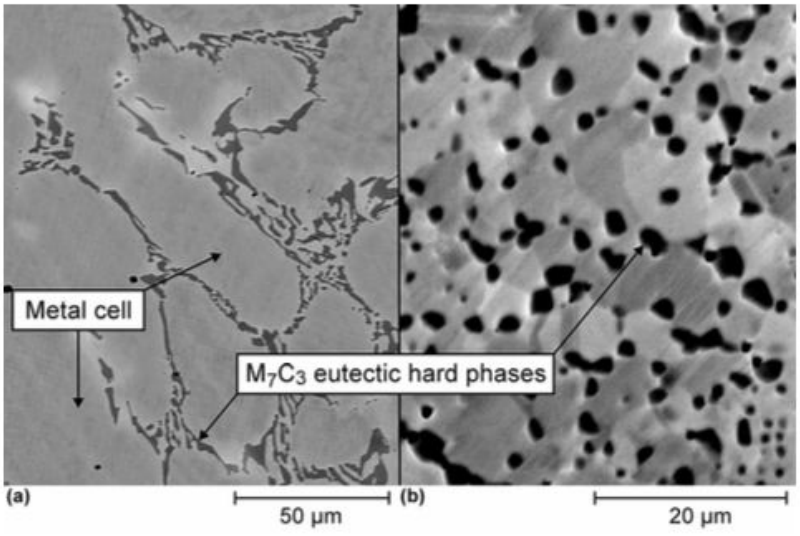

Figure 7: Stellite 6 microstructure in the (a) as-cast and (b) hot isostatic pressed conditions.

3.4.B - Application Method

Stellite alloys can be applied using fusion welding and, less commonly, brazing. To prepare for brazing, substrate material must be thoroughly cleaned and brazing flux applied. Joining can be done using torch or induction brazing with silver, gold, palladium, or nickel-based alloys. The assembly is then pressed together to squeeze out excess flux and still air cooled. High temperature brazing is usually done in a furnace. The fusion welding is done using gas tungsten-arc (TIG) with argon flow of 25 CFH, gas metal-arc (MIG), shielded metal-arc (coated electrode), and oxy-acetylene, in that order of preference. The Stellite alloy is typically preheated and maintained at 1000 °F to prevent cracking, then still air cooled. INCONEL 82, 92, or 625 filler metal is recommended to join Stellite to softer substrates such as carbon steel or stainless steel (Kennametal 2013).

3.4.C - Adhesion to Carbon Steel Pipes and Intricate Parts

Proper coating adhesion is dependent on the quality of the application process. During the welding process, high thermal energy leads to partial melting of the substrate material and dilution with the coating. Although adhesion and diffusion between coating and substrate is desirable, dilution can change the mechanical properties of the coating; therefore, dilution should be minimized or additional layers of coating added. There is a risk of stress-induced cracking due to the hard phases in the Stellite which may lead to delamination. To prevent stress-induced cracking, a tough intermediate buffer layer can be applied to the substrate material (Theisen 2017).

3.4.D - Erosion Resistance

Stellite 6B is designed to combine toughness and wear resistance to perform under harsh, high temperature erosive conditions. To accomplish these properties, Stellite 6B undergoes hot working and solution heat treating. Reported tensile strength, elongation, and hardness values are 896 MPa, 7% MIN, and 33-43 HRC, respectively. Average abrasive wear data collected for Stellite 6B measured 8.2 mm^3 volume loss when test specimens were ground against a sand abrasive wheel, compared to a 37.2 mm^3 volume loss for quench and tempered 1090 steel (55 HRC) under the same conditions (Kennametal 2013). Further data was presented by Kennametal indicating superior abrasion resistance compared to stainless steel (Figure 8).

Average Abrasive Wear Data

ALLOY	CONDITION	VOLUME LOSS, mm^3	HARDNESS, ROCKWELL	WEAR COEFFICIENT[1]
Stellite™ 6B	Mill annealed	8,2	C–38	0,471 x 10^{-3}
Stellite™ 6K	Mill annealed	13,3	C–46	0,946 x 10^{-3}
Stellite™ 25	Mill annealed 1 hr. at 1600°F (871°C)	53,0	C–24	2,00 x 10^{-3}
1090 Steel	Water quenched + 4 min. at 900°F (482°C)	37,2	C–55	8,00 x 10^{-3}
Type 316 Stainless Steel	As received sheet	81,4	B–86	2,0 x 10^{-3}
Type 304 Stainless Steel	As received sheet	102,1	B–92	3,00 x 10^{-3}

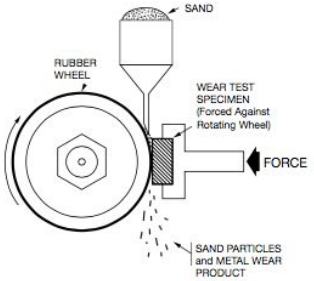

Figure 8: Three-body abrasion data for Stellite 6 alloys compared to steel alloys reported by Kennametal. .

Additional erosion data from literature was obtained for validation using solid particle impingement test G76 which more closely mimics erosion due to catalyst flow. Research done though the American Society of Mechanical Engineers for the 17th Annual North American Waste-to-Energy Conference used bed ash from an operating boiler (silicon and calcium) as the erodent with a 556 µm particle size and 141.2 ft/s (40 m/s) particle velocity for a 3 hour test duration on various coatings. (Table

II). The results showed impressive performance from Conforma Clad, a WC-based coating (Dooley 2009).

Table II: Solid Particle Erosion Data for Various Coatings

Material	Thickness Loss (cm/g)*10^{-6}	Impingement Angle	Temp (Deg F)
Conforma Clad	23	90	900
Inconel 625	54	90	900
Inconel 622	56	90	900
309 SS	91	90	900
Stellite 6	185*	90	Ambient
Amstar 880	210*	90	Ambient

3.5 Selection of Potential Alternative Coatings to Stellite

3.5.A - Conforma Clad

Indication of the high performance of the WC cladding, under the brand name Conforma Clad, based on literature as well as its possible use by Exxon Mobil in FCC units, makes this a coating of interest. The cladding consists of about 50% WC particles embedded in a Ni alloy matrix (Table III). This classifies the material as a metal matrix composite (MMC). Cemented carbide cermets typically have a higher WC composition and use cobalt as a binder.

Table III: Conforma Clad Compositions

Cladding Composition (Weight Percentage)			
	WC 200	WC 210	WC 219
Tungsten Carbide*	62%	55%	48%
Nickel	30%	34%	39%
Chromium	6%	7%	8%
Other	2%	4%	5%

The hard WC particles help provide resistance to abrasion while the metal matrix helps increase fracture toughness. The hard phase in the MMC can be optimally adjusted based on the attacking abrasive particle. Relative to the attacking abrasive, the hard phase should be more hard and equal in size or larger. Finely dispersed hard particles best resist indentation and coarse abrasives.

The cladding properties show high density, low porosity, high hardness, and a bond strength slightly higher than the tensile strength of normalized steels (Table IV). These properties indicate sufficient adhesion and coating density potential (Kennametal 2014).

Table IV: Conforma Clad Mechanical Properties

Cladding Properties			
	WC 200	WC 210	WC 219
Density (lb/in^3)	0.44	0.42	0.40
Thermal Conductivity (BTU in/h•ft^2•°F)	230	200	170
Metallurgical Bond Strength (psi)	>70,000	>70,000	>70,000
Porosity	<3%	<3%	<3%
Rockwell Hardness (HRC)**	64–70	60–66	56–62

The processing of Conforma Clad involves mixing powders to the proper composition for the type of cladding, rolling the powder to the proper thickness to form a flexible cloth, applying the cloth to a substrate coated with adhesive, and furnace brazing at temperatures above 1000 °C to melt and sinter the coating to form a metallurgical bond with the substrate (Figure 9). This results in a coating thickness around 2mm. The flexibility of the cloth overlay increases the practicality of coating more intricate geometry (Wiltz 2011).

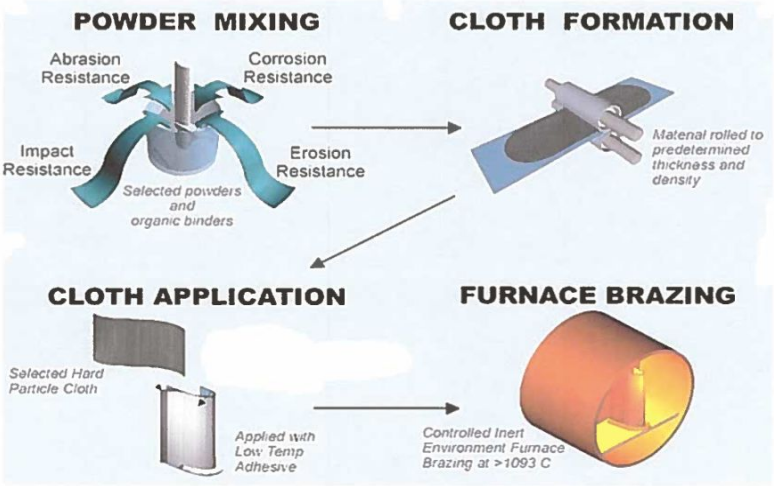

Figure 9: Conforma Clad coating application process.

Further industry data comparing ASTM G76 solid particle erosion of Conforma Clad and other coatings indicate the potential for WC claddings to outperform Stellite under harsh erosive conditions (Figure 10) (Wiltz 2011).

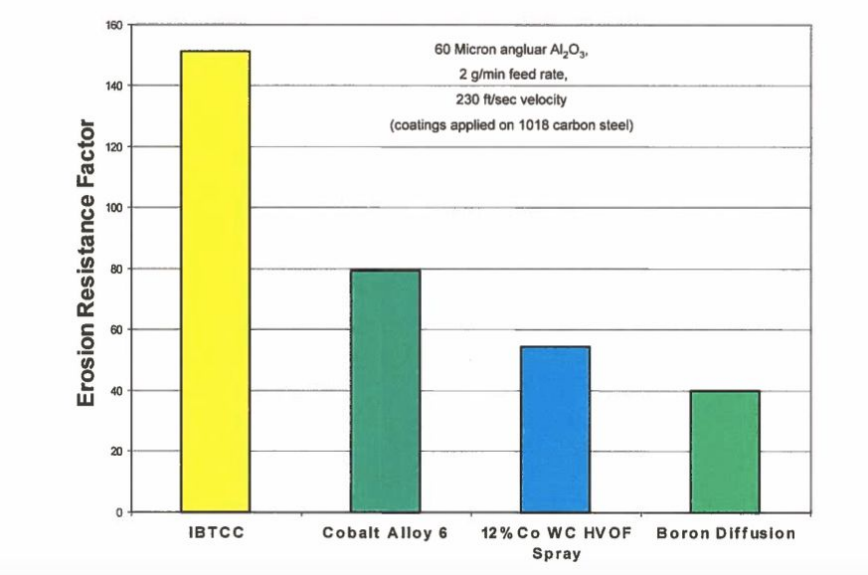

Figure 10: Solid particle erosion data from the Exxon Mobil pumping service wear case study investigating protective coatings for extreme erosive conditions showing impressive results for infiltration brazed tungsten-carbide cladding or Conforma Clad.

3.5.B - Hardide Coating

A unique variety of WC coatings are produced by Hardide, utilizing chemical vapor deposition (CVD) to produce a nanostructured WC in a tungsten matrix, with no other binder material, forming a coating about 50 µm thick. The CVD process involves exposing the substrate to a gas phase of the coating material (tungsten and carbon) that deposits atom-by-atom onto the substrate to form a dense coating with a grain structure in the nanometer length scale (Figure 11). The most widely used Hardide coating, Hardide-T, offers increased toughness as well as high hardness due to WC inclusions about 1-10 nm in size.

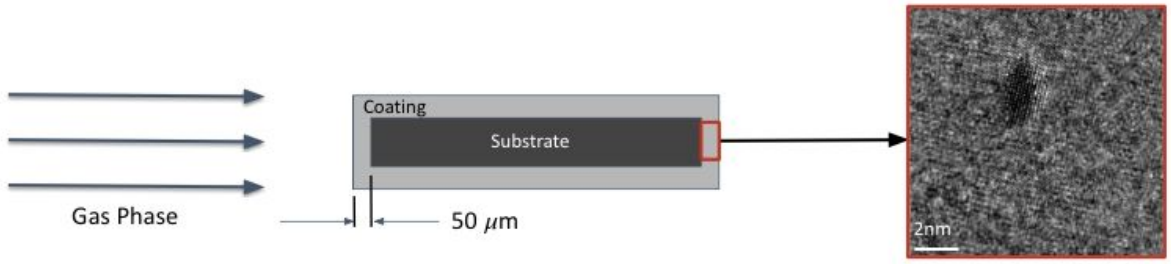

Figure 11: Simplified chemical vapor deposition process for the application of the nanostructured WC-W Hardide coatings, showing a high resolution electron microscopy image of a WC precipitate in a Hardide-T coating.

CVD Hardide coatings are measured to have a porosity of less than 0.04% and a hardness of 1000 HV or more. Adhesion testing using ASTM C633 indicated that Hardide coatings have a bond strength of greater than 10,000 psi, achieving the limit of the epoxy adhesive used for the test. CVD coatings are of benefit not only because of high density but also due to the ability to fully coat extremely intricate geometries. Reported solid particle impingement erosion data for Hardide coatings claim superior resistance compared to WC claddings with lower volume loss per gram of abrasive even at 90° impingement angles (Table V) (Zhuk 2010).

Table V: Comparison of Erosion Data for WC-W coatings and Other Erosion Resistant Coatings

Angle of target, °	Erosion Rate, $mm^3/g*1000$					
	CVD Tungsten Carbide coating	Chrome Carbide Weld Overlay	White Iron	Abrasion-resistant steel	WC cladding	Hard Chrome
30	17					
45	19	71	76	53	36	25
60	18	66	64	48	41	26
90	18	60	40	40	50	30

Erosion and wear testing has a great deal of variability in terms of impingement angle, particle size, particle velocity, and testing duration. This makes it difficult to cross compare test results. It is most practical for an erosion test to be conducted on all coatings of interest using the same parameters that mimic erosion conditions for a specific application. With all the new advancements in coating materials and application methodology, it has become necessary to re-evaluate currently used methods for erosion protection. It is also significant to consider the properties of a material subject to erosion since brittle and ductile materials undergo different erosion failure mechanisms. To confirm whether or not Stellite is the optimal choice for continued use at Chevron refineries, it is necessary to further investigate the performance of promising alternative coatings, such as WC-based coatings.

3.6 Problem statement

An alternative erosion resistant coating such as Conforma Clad and Hardide-T is needed to meet or exceed the erosion resistance of Stellite on A36 steel as measured by solid particle impingement, hardness, and adhesion.

4. Experimental Procedure

4.1 Methodology for Project Designs

4.1.A – Design Criteria

The priority testing was to determine the rate of erosion of a coated carbon steel coupon subjected to solid particle impingement using gas jets as specified by ASTM G76 (ASTM 2018). Other relevant properties include hardness and adhesion of the coating. Hardness is a mechanical property directly related to the ability of the material to withstand particle impingement and wear from moving particles. The quality of adhesion of the coating to the steel coupon will give insight into how successful the coating inevitably will be at protecting the steel surface. The currently used erosion resistant coating, Stellite, was intended to be used comparatively; however, it was not delivered by Kennametal per our request. Design criteria was determined by direct information from Chevron ETC related to the environment within an FCC unit transporting catalyst. Success was measured by the ability of obtained data to predict the erosion resistance of selected coatings relative to Stellite applied in an FCC unit. At least 2 repetitions are required to conduct statistical analysis, but more than 2 repetitions are preferred. The final data was the volume loss of material per unit mass of abrasive (mm^3/g).

4.1.B – Variables

Variables included the type of coating, particle impingement angle, particle impact velocity, specimen standoff distance, and characteristics of the abrasive material such as particle size and composition. Temperature was another variable of interest that could be accounted for using ASTM G211-14; however, elevated temperatures were not investigated in this experiment.

4.1.C - Others

Required Testing Supplies:

- Sand-Blasting Apparatus
- A36 Mild Steel
- Conforma Clad WC219 and WC210
- Hardide-T CVD Coating
- Mass-Balance Scale
- Personal Protective Equipment

Chevron ETC provided funding for this project. Items were reviewed and approved by the project advisor as well as Chevron personnel involved with the project. Designated lab space to store the sand

blasting apparatus and supplies was necessary. It also was necessary to work with other students and faculty to schedule use of the SEM and hardness testing machinery.

4.2 Methodology for Experiments and Testing

4.2.A – Inputs

The factors of interest for this experiment were the particle angle of incidence, change in mass of coating, and time. The latter factors are all parametric, as some were fluctuated to simulate catalyst flow at different angles of impingement. Each coating tested (A36 Steel, Conforma Clad, and Hardide-T) were applied to A36 steel coupons and subjected to particle impingement at four constant time intervals at incident angles of 90° and 25° (Figure 12). All coatings were subjected to 70 µm alumina particle blasting. The time intervals were 60, 120, 180, and 240 ± 0.5 seconds for 90° impingement at an abrasive mass flow rate of 1.2 g/s with 3 repetitions of the test. At the 25° impingement angle, the time intervals were 105, 210, 315, and 420 ± 0.5 seconds at an abrasive mass flow rate of 0.5 g/s with 2 testing repetitions. After each time interval, the test specimen was weighed to determine mass loss of the selected coating.

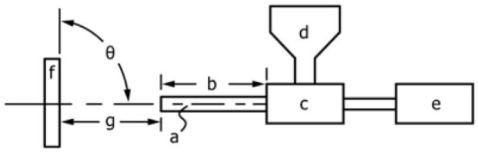

where:

a = gas jet nozzle,
b = nozzle length,
c = mixing chamber,
d = abrasive hopper,
e = gas source,
f = test specimen,
g = nozzle-to-specimen distance, and
θ = impingement angle.

Figure 12: Test apparatus utilized to determine erosion rates.

Each carbon steel sample was approximately a 1x3x0.25 inch coupon, with varying coating thicknesses. Each coating had a fresh coupon tested for each of the four time intervals stated above, totaling 12 trials for the 90° impingement and 8 trials for the 25° impingement (ASTM 2018).

4.2.B – Outputs

Mass loss was chosen as the primary response variable because this most accurately addressed the problem statement, considering erosion resistance was the focus of this research. The mass of each coating was weighed on an analytical balance, Minus k Technology BM-8 bench top vibration isolation

platform, to ± 0.0001 g before erosion, and at the end of each time trial. Time was measured utilizing a stopwatch accurate to 0.01 seconds. Mass and time for each sample was plotted to obtain the erosion rates (Figure 13). The reported average erosion value was obtained by dividing the average erosion rate by the density of the eroded material and the abrasive mass flow rate.

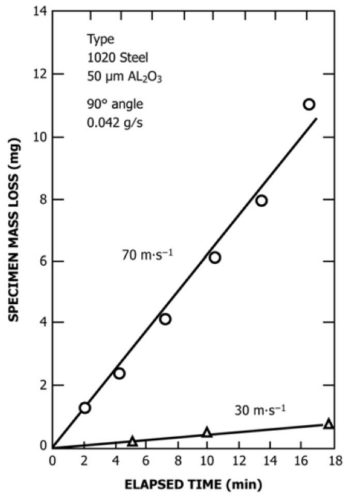

Figure 13: Mass loss versus time utilized to determine erosion rate (ASTM 2018).

Outputs are both quantitative and qualitative. The quantitative measures of erosion values were analyzed statistically to determine the performance of each coating. Erosion value standard deviations from the mean (A36) displayed how well each coating combats erosion. The quantitative erosion analysis interacts qualitatively based on how well each coating performed.

4.2.C – Experimentation

Safely conducting the erosion testing was our top priority. The following personal protective equipment (PPE) was used: rubber gloves for abrasion damage, safety glasses to shield eyes from particles, and a dust mask to prevent inhalation of particles.

ASTM - G76 Conducting Erosion Tests by Solid Particle Impingement Using Gas Jets was pertinent to our project. The above testing parameters, and specifications were determined by this standard. If any deviation from the standard is needed, specific details will be explained and noted.

The erosion testing was block tested, as described in section 4.2.A. Each coating was subjected to particle impingement at four distinct times, and two different impingement angles. If a trial did not provide sufficient results, then retesting occurred. Scanning electron microscopy (SEM) and optical microscopy was utilized to inspect the coatings before and after erosion testing for characterization.

Hardness was recorded via Rockwell hardness scale HRB and HRC to determine hardness correlation with measured erosion rates and validate industry data and processing methods.

Standard deviation and ANOVA statistical methods were utilized to rate each of the coatings against A36 Steel. Each coating plot was superimposed on a single mass loss versus time plot to compare erosion ratings (Figure 4).

5. Results and Discussion

5.1 Results: 90° Impingement, 95 psi Compressed Air Pressure, 1.2 g/s Mass Flow Rate

Post-erosion testing, the sample coupons were lined up side by side to compare their eroded surfaces (Figure 14). Surprisingly, A36 steel samples displayed the least amount of material loss. Conversely, the Conforma Clad WC219 and WC210 coupons displayed the most severe material loss. This was depicted when observing the erosion zones at each time and comparing them to the A36 reference coupons. Both Conforma Clad coatings had deep dimple rupture surfaces at each impingement time.

The Hardide-T chemical vapor deposited coatings were fully penetrated at the lowest impingement time of 60 seconds. This dilemma led to inconclusive data for the Hardide-T coupons, as both the coating material and A36 steel substrate material was eroded away. With both simultaneously eroding, the mass loss of the coating itself could not be measured.

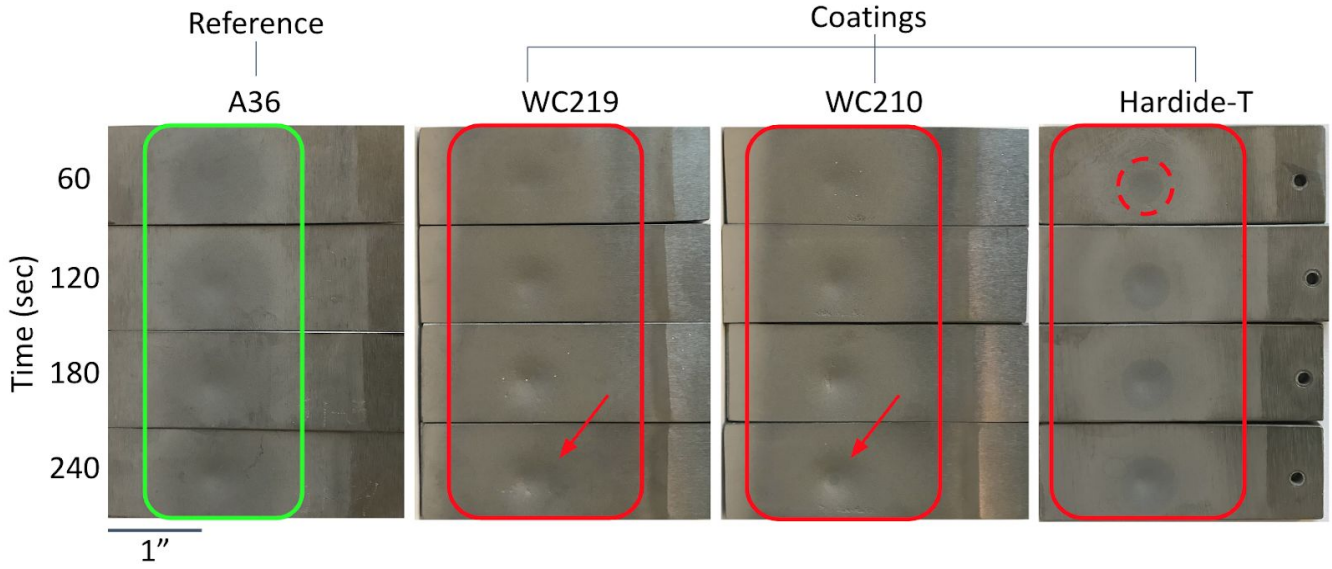

Figure 14: Single sampling of one-time group of A36 reference steel, along with WC219, WC210, and Hardide-T coatings after distinct impingement times and a 90° impingement angle.

The average mass loss of each sample was plotted versus their corresponding impingement times to determine the erosion rate of each material from the slope of the plots (Figure 15). Standard deviation error bars were used to statistically determine the test method repeatability. Near unity R^2 values suggested testing repeatability. The Hardide-T coating displayed a similar erosion rate to the bare A36 steel. This was a result of the thin coating being fully penetrated, leading to the removal of the A36 steel substrate.

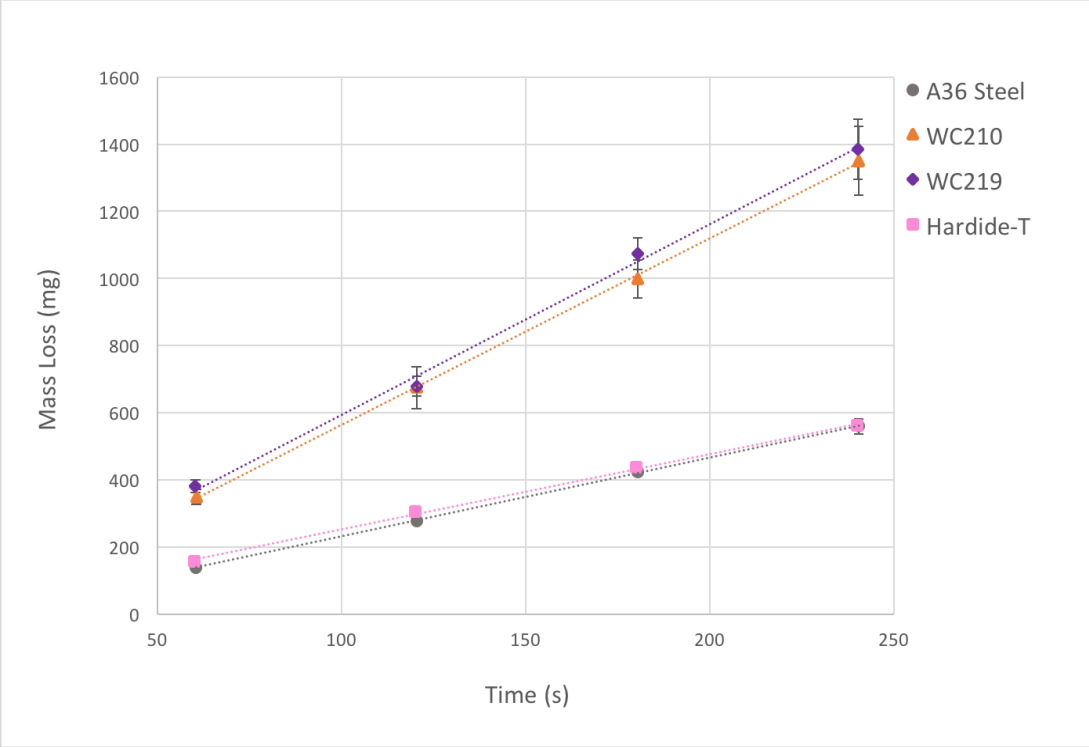

Figure 15: Erosion plots of tested samples with standard deviation error bars, graphically displaying the A36 steel eroding at a lesser rate than Conforma Clad WC210 and WC219.

The average erosion rate of the A36 steel coupons was 2.3433 mg/s, which was 58% less than both WC219 and WC210. Both Conforma Clad coatings displayed similar average erosion rates of 5.677 and 5.5482 mg/s respectively. Taking into consideration the density of the eroding material as well as the mass flow rate, average erosion rates were converted to average erosion values (Figure 16). The erosion value is a measure of volume loss of material per gram of abrasive. A36 steel yielded an average erosion value of 0.251 mm^3/g, while WC219 and WC210 had similar values of 0.428 & 0.398 mm^3/g respectively. The average erosion values reinforced the trends seen in the average erosion rate data (Table VI).

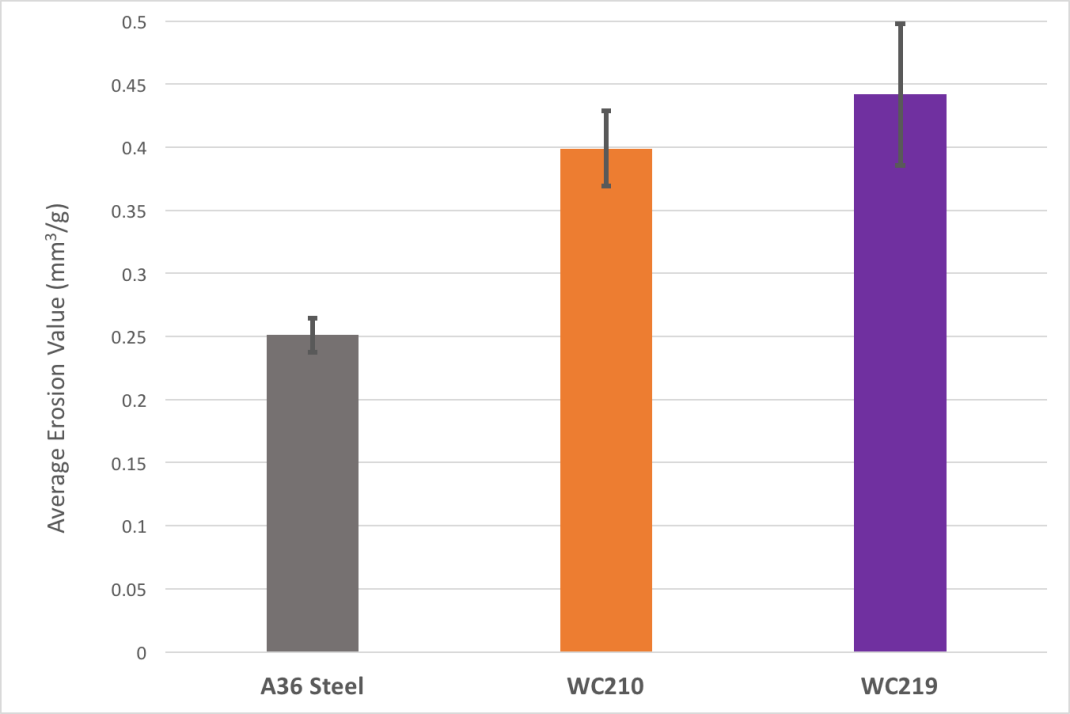

Figure 16: Visual representation of average erosion values for A36 steel, WC219, and WC210 at a mass flow rate of 1.2 g/s and 90° impingement angle.

Table VI: Average Erosion Rate, Value, Standard Deviation, and R^2 of A36 Steel, WC219, and WC210

Material	Average Erosion Rate (mg/s)	Standard Deviation	Average Erosion Value (mm^3/g)	Standard Deviation	R^2
A36 Steel	2.3433	0.1273	0.251	0.0136	0.99979
WC219	5.6777	0.7421	0.428	0.0560	0.99707
WC210	5.5482	0.4148	0.398	0.0298	0.99967

One-way ANOVA testing was conducted to compare the mean erosion values for A36 steel, WC219, and WC210. Hardide data was not included due to the rapid breakthrough of the coating leading to invalid results. The resulting P-value of 0.0019 indicated that at least one of the means was different than the others. A pooled standard deviation interval plot showed that the mean erosion value for A36 steel was different from the values for both claddings, which were not different from each other, with 95% confidence (Figure 17).

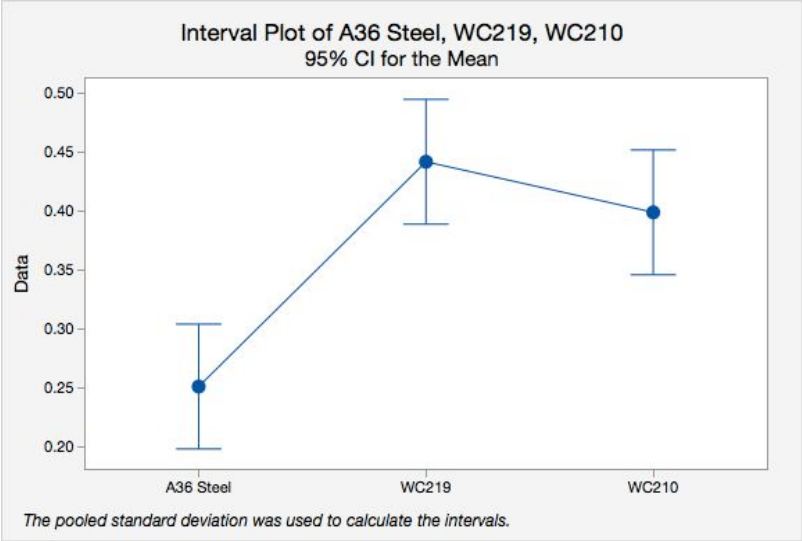

Figure 17: One-way ANOVA statistics of mean erosion values for A36 steel, WC219, and WC210 at 90° impingement.

Initially, the erosion rates calculated from our test data were surprising, as we expected the WC claddings to have a lower erosion rate than bare A36 steel. After reviewing literature, we can begin to speculate the cause of these results. Due to their brittle nature, the Conforma Clad coatings experienced higher amounts of mass loss at higher angles, due to fracture mechanisms. Conversely, the more ductile A36 steel was less susceptible to mass loss at oblique impingement angles. This can be seen graphically from Figure 6 in section 3.2.

In an effort to understand our results from erosion testing, optical microscopy was used to help determine how the structure of our materials affected their erosion resistant performance. Prior to erosion testing, the interface of each coating was examined to determine which phases were present in our materials as well as the adhesion to the substrate materials.

Both Conforma Clad WC210 and WC219 micrographs had similar results. The claddings displayed a high concentration of WC particles surrounded by a Ni-matrix (Figure 18). There was a distinct interface segregating the claddings from the A36 substrate. No signs of microvoids or delamination were seen, suggesting that the adhesion between the two materials was optimized by the cladding process. Another take away from these micrographs was the microstructure of the A36 steel used for the experiment. The A36 steel displayed large pearlitic regions, nucleated at prior austenite grains, surrounded by an alpha-ferrite matrix. It was deduced that the reference substrate material selected was properly heat treated to conform to the ASTM A36 designation. The steel closer to the interface zone may have been affected by the high temperature brazing process, which was displayed by the coarsened grain regions. This region is typical near the weld-zone for steels. The microstructure also suggested that the

composition and processing did not have a significant role in why the bare steel coupons were eroded at a lower rate than the WC claddings.

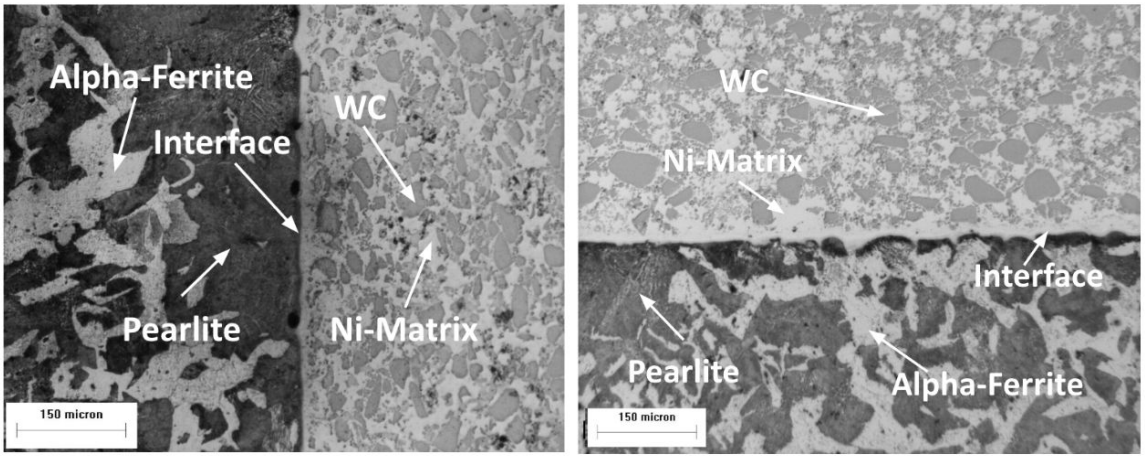

Figure 18: Micrographs of Conforma Clad WC210 (left) and WC219 (right), illustrating present phases and optimal adhesion between the different materials.

A micrograph of a Hardide-T chemical vapor deposited WC coupon was also taken prior to erosion testing. The WC-W coating was relatively thin, about 50 ± 15μm, confirming Hardide's specification of the coating thickness (Figure 19). The thinness of the coating partially explained why it was fully penetrated at the lowest impingement time of 60 seconds. There was also a thin proprietary material, observed at the interface, which allowed the coating to adhere to the A36 steel substrate. Similar to the Conforma Clad coupons, no microvoids or signs of delamination were inspected, suggesting optimal adhesion between the two different materials. The steel microstructure was more refined relative to the Conforma Clad coupons.

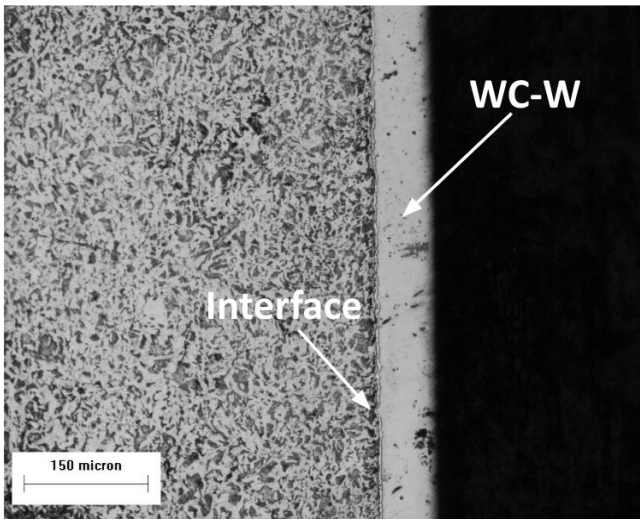

Figure 19: Micrograph of Hardide-T CVD coating, illustrating a refined A36 steel structure adhered to the coating.

This may be a direct result of the different process by which the Hardide-T coating was applied. The CVD process did not introduce a high thermal cycle, which did not alter the original microstructure of the steel.

Post-erosion testing, micrographs of WC219 and WC210 coupons eroded at the longest impingement times of 240 seconds were taken. Both claddings displayed similar images. Both interfaces appeared to be intact, indicating that erosion testing had no effect on adhesion (Figure 20). Notably, there appeared to be a high volume of microvoids on the eroded surfaces of the claddings. It was likely that the 70 μm Al_2O_3 particles eroded the Ni-matrix binder rapidly, removing the binder from supporting the WC particles suspended. Without the Ni-matrix, the particles were readily able to dislodge upon some impact. Since there was about a 50% concentration of WC particles that could flake away, Conforma Clad coatings had a much higher mass loss than the bare A36 steel, resulting in relatively higher erosion rates.

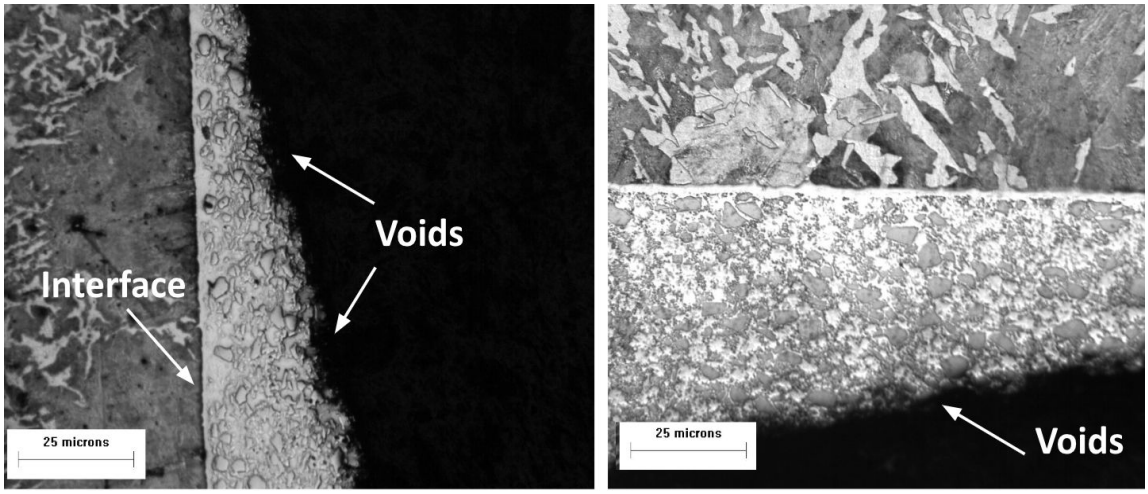

Figure 20: Micrographs of WC210 (left) and WC219 (right) post-erosion testing, displaying a high volume of microvoids resulting in a relatively high erosion rate.

In addition to optical microscopy, scanning electron microscopy was used to gain a similar perspective of the adhesion between the selected WC coatings. The scanning electron images fortified that the adhesion between the Hardide-T coatings and WC Claddings were optimal. The SEM images displayed no signs of delamination or voids (Figure 21). SEM imaging of the WC cladding eroded surface indicated faceting and quasi-cleavage, likely from the failure of the Ni-matrix and loss of WC particles, similar to the A36 steel eroded surface (Figure 22).

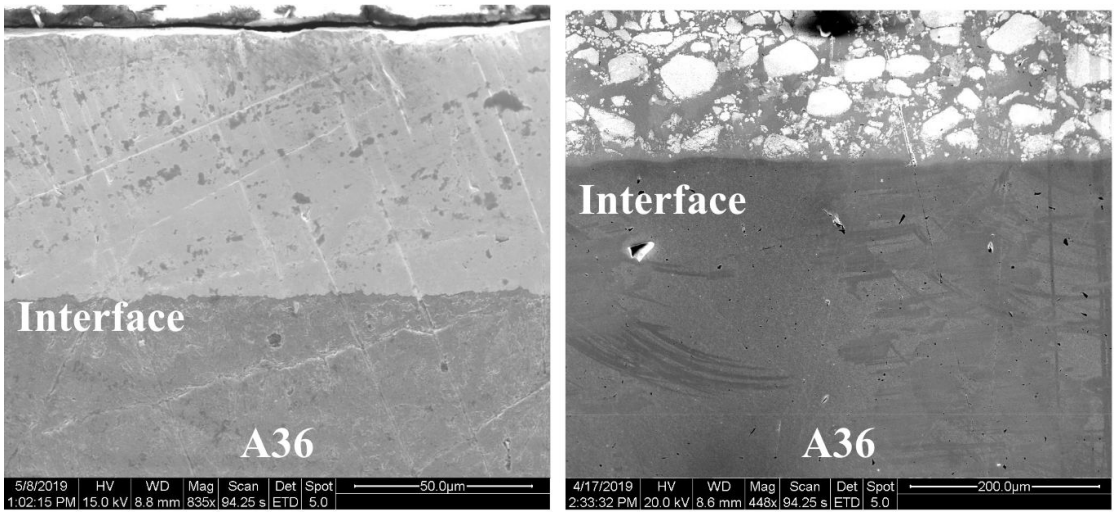

Figure 21: Scanning electron images of Hardide-T (left) and WC210 (right) interfaces adhered to A36 mild steel.

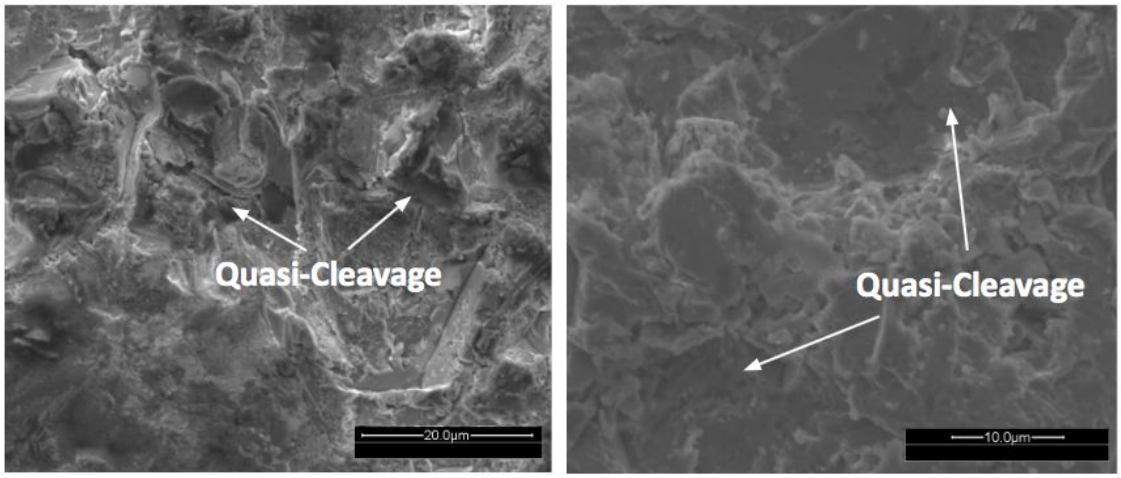

Figure 22: SEM images of eroded surfaces of WC210 (left) and A36 steel (right) showing indications of quasi-cleavage.

Hardness values of each material were used to compare the coatings and validate industry claims (Table VII). As expected, A36 steel displayed the lowest hardness with an average of 72.23 HRB as-received. Hardide-T was the second lowest at 82.81 HRB, which was about 13% higher than A36 steel. We believe the hardness of the CVD coating resembled the A36 bare steel, due to penetration into the steel beneath the coating during Rockwell hardness testing. To obtain more accurate readings, microhardness testing could have been performed. The Conforma Clad WC210 and WC219 average hardness values were similar, at 58.93 and 55.59 HRC, respectively, with a 6% difference. The average hardness values of the materials provided confirmation of the ductile and brittle characteristics of each material type.

Table VII: Average Hardness of Materials Tested

	A36 Steel		WC210		WC219		Hardide-T
	As-Received	Eroded	As-Received	Eroded	As-Received	Eroded	As-Received
Average	72.23 HRB	70.55 HRB	58.93 HRC	54.44 HRC	55.59 HRC	45.15 HRC	82.81 HRB
Standard Deviation	2.24	2.65	5.2	5.01	2.37	16.08	1.47

5.2 Results: 25° Impingement, 40 psi Compressed Air Pressure, 0.5 g/s Mass Flow Rate

After 90° erosion testing, it was determined that the angle was too severe for the WC-W coatings, so the impingement angle was reduced to about 25° to understand how all testing materials would withstand a lesser angle of impact as well as to obtain usable data for Hardide-T. At a lower impingement angle, the A36 bare steel eroded at the highest rate, while the Hardide-T and WC210 eroded at lower rates (Figure 23). WC219 was not re-tested due to its similarity to WC210. The resulting average erosion rates fortified that ductile materials experience a higher mass loss, while brittle materials experience a relatively lower mass loss at lower angles.

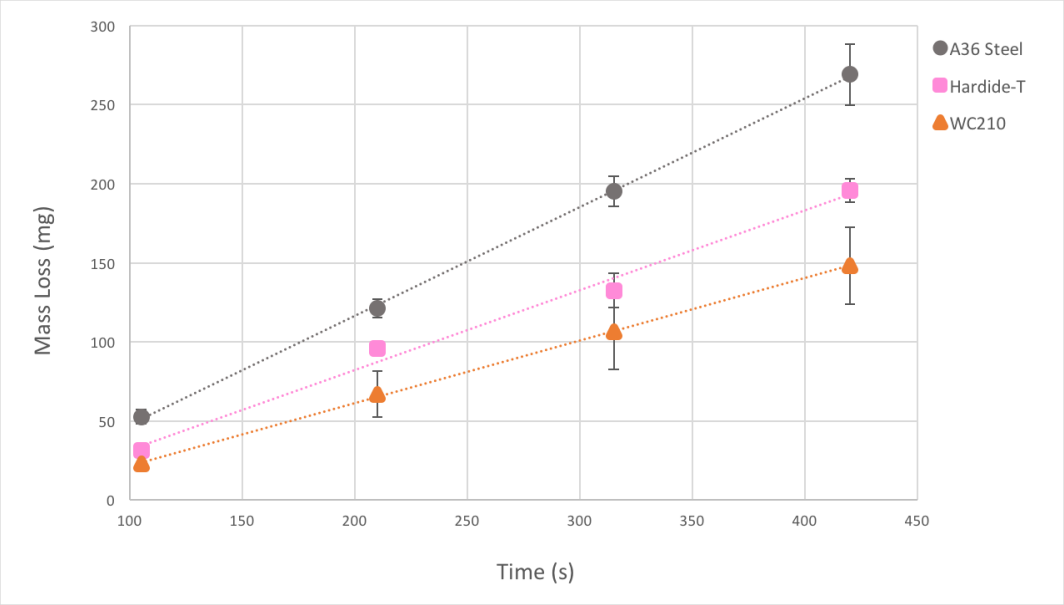

Figure 23: Erosion plot of A36 steel, Hardide-T, and WC210 eroded at 25°.

Conversion of average erosion rates to average erosion values changed the ranking of Hardide-T to appear to erode slightly less than WC210 due to the high density of Hardide-T with a value of 19 g/cm^3 compared to WC210 with a density of 11.6 g/cm^3. A36 steel still appeared to clearly have the highest

erosion value (Figure 24). Standard deviation and R^2 values for the average erosion rates and the standard deviation values for the average erosion values again indicated testing repeatability (Table VIII).

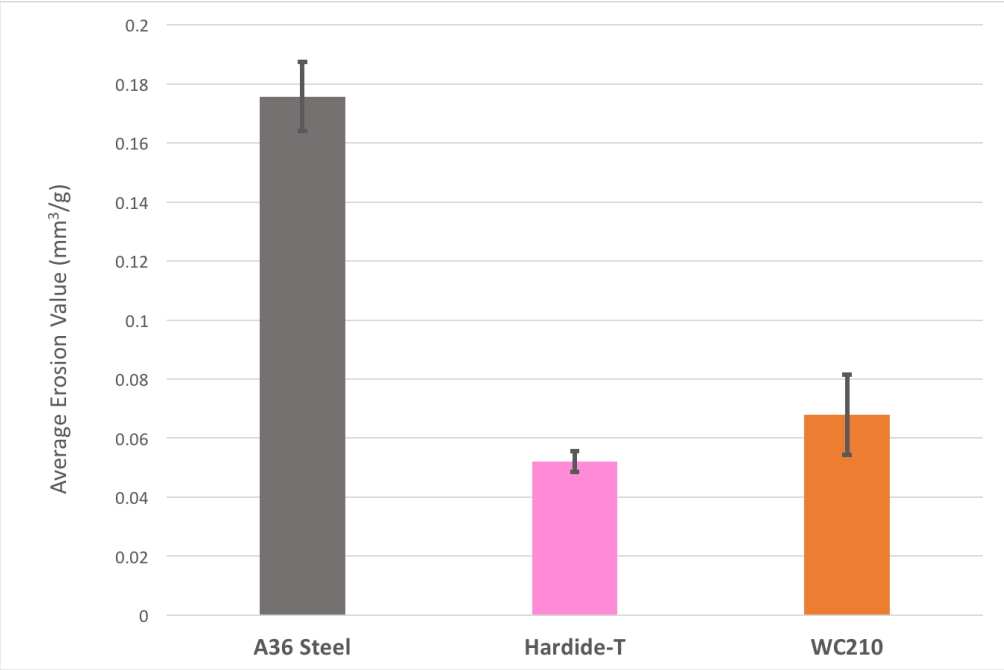

Figure 24: Visual representation of average erosion values for A36 steel, Hardide-T, and WC210 at a mass flow rate of 0.5 g/s and 25° impingement angle.

Table VIII: Average Erosion Rate, Value, Standard Deviation, and R^2 of A36 Steel, Hardide-T, and WC210

Material	Average Erosion Rate (mg/s)	Standard Deviation	Average Erosion Value (mm^3/g)	Standard Deviation	R^2
A36 Steel	0.6887	0.0461	0.1757	0.0118	0.99967
Hardide-T	0.5049	0.0339	0.0521	0.0035	0.98957
WC210	0.3966	0.0795	0.0679	0.0136	0.99956

One-way ANOVA statistics were calculated using the mean erosion values for A36 steel, Hardide-T, and WC210. The resulting P-value of 0.0025 indicated that at least one of the means was different than the others. Using pooled standard deviation (Figure 25), it was determined that A36 steel had a higher average erosion value than Hardide-T and WC210, which did not have means values different from each other, with 95% confidence.

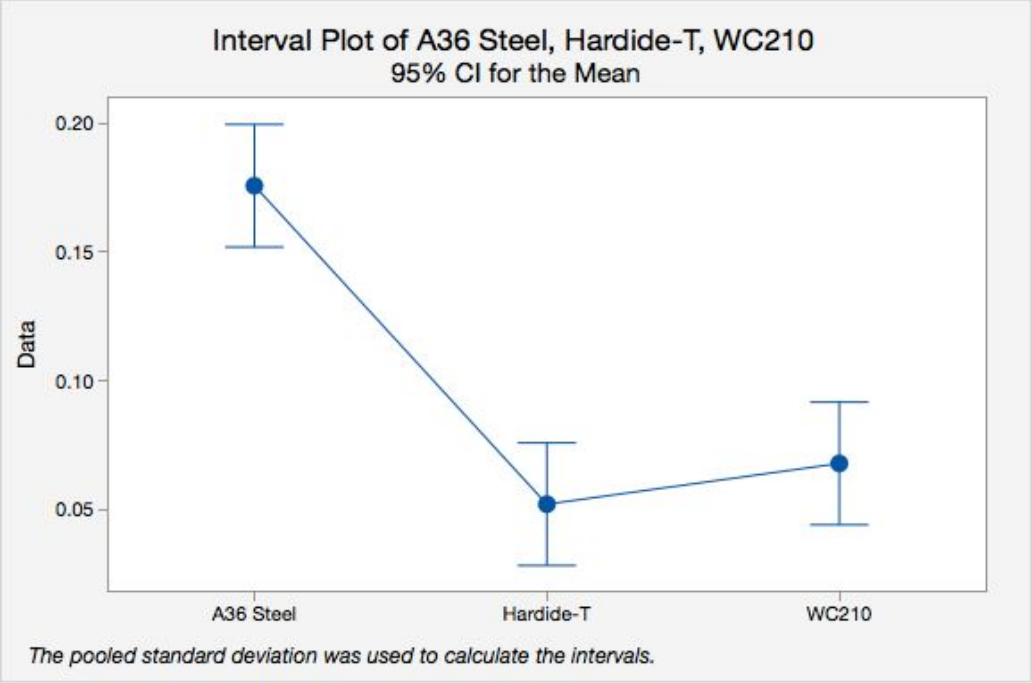

Figure 25: One-way ANOVA results for mean erosion values of A36 steel, Hardide-T, and WC210 at 25° impingement.

The results obtained can be used to verify that WC-based coatings and A36 steel follow the trends seen for brittle and ductile materials subjected to erosive conditions, including those mimicking erosion due to catalyst flow. The 90° impingement angle, with relatively high mass flow rate, compromised the more brittle WC claddings and WC-W CVD coatings. However, the 25° impingement angle at a lower mass flow rate spared the coatings while severely attacking the ductile steel. This reveals that complex micromechanics are at work at the material level. This information can be translated to design recommendations including use of hard coatings for pipes experiencing mostly abrasion while increasing material or coating thickness in areas of 90° impingement. It may also be beneficial to stack coating at more severe angles of impact.

6. Conclusions

1. At the highest impingement angle and mass flow rate, the average erosion value of bare A36 steel was less than both WC claddings with 95% confidence

2. At a lower impingement angle and mass flow rate, the average erosion values of Hardide-T and WC210 were less than that of A36 steel with 95% confidence

3. Near unity R^2 values and low variance indicated testing repeatability

4. Unexpected results were obtained at the highest impingement angle and mass flow rate due to aggressive dislodging of WC particles from loss of Ni-Matrix binder

5. Small Hardide-T thickness compromised erosion rate data collection at the highest impingement angle and mass flow rate

7. Future Work

- Investigate and test other types of erosion-resistant coatings including a Stellite reference
- Develop a method to measure particle velocity
- Conduct more test repetitions
- Vary angle of impingement
- Account for elevated temperature conditions

8. References

AAPG. *Petroleum Through Time*. Petroleum Geology. https://www.aapg.org/about/petroleum-geology/petroleum-through-time/what-is-petroleum

Adler, T. U.S. Department of Energy. *Erosive Wear Failures*. ASM Handbook. Volume 11: Failure Analysis and Prevention. pg 995-1001. 2002.

Ancheyta, J. *Petroleum Refining. In Modeling and Simulation of Catalytic Reactors for Petroleum Refining*. Hoboken, NJ, USA: John Wiley & Sons. pg 1-52. 2011.

ASTM Standard G76-18. Standard Test Method for Conducting Erosion Tests by Solid Particle Impingement Using Gas Jets. ASTM International, West Conshohocken, PA. 2018. DOI: 10.1520/G0076-18. www.astm.org.

Cotell, C.M. Sprague, J.A. Smidt, Jr. *Overview of Wear and Erosion Testing*. ASM Handbook. Volume 5: Surface Engineering. pg 679-680. 1994.

Davis, J.R. *Corrosion: Understanding the Basics.* ASM International. 2000.

Dixon, R. Chen, S.P. Los Alamos National Laboratory. *Fundamentals of Metal and Metal-to-Ceramic Adhesion*. ASM Handbook. Volume 6: Welding, Brazing, and Soldering. pg 143-149. 1993.

Dooley, R. Wiertel, E. *A Survey of Erosion and Corrosion Resistant Materials being used on Boiler Tubes in Waste to Energy Boilers*. Proceedings of the 17th Annual North American Waste-to-Energy Conference. ASME. 2009.

Kennametal Application Bulletin. *Standard Conforma Clad Tungsten Carbide Formulations - Power Generation*. 2014.

Kennametal Brochure. *Wrought Wear-Resistant Alloys*. Stellite 6B and 6K. www.kennametal.com/stellite. 2013.

Kennametal. *Stellite Alloys*. http://www.stellite.com/en/products/stellite-family/stellite-family-stellite.html

Lee, D. Kennametal Stellite. *Wear-Resistant Coatings*. ASM Handbook. Volume 5A: Thermal Spray Technology. 2013.

Murphy, Martin A. *Analysis, calculation techniques predict FCC erosion and fluidization*. Oil & Gas Journal. Feb 21, 1994. 92. 8. pg 54.

Theisen, W. Rottger A. Bochum, R. *Carbide- Boride-Based Thick Coatings for Abrasive Wear-Protection Applications*. ASM Handbook. Volume 18: Friction, Lubrication, and Wear Technology. pg 597-613. 2017.

Vogt, E.T.C. Weckhuysen, B.M. *Fluid Catalytic Cracking: Recent Developments on the Grand Old Lady of Zeolite Catalysis*. Royal Society of Chemistry. Chem. Soc. Rev. 2015. 44. 7342. DOI: 10.1039/c5cs00376h.

Wikipedia contributors. *Chevron Corporation*. Wikipedia, The Free Encyclopedia. 9 June 2019.

Wikipedia contributors. *Fluid catalytic cracking*. Wikipedia, The Free Encyclopedia. 17 May 2019.

Wiltz, T. Hertel, D. Kinball, D. Newman T. Zielewski, C. *Wear Reducing Technology Newly Applied to Severe Pumping Services*. TAMU Case Study. 2011.

Wood, R. University of Southampton. *Solid Particle Erosion*. ASM Handbook. Volume 18: Friction, Lubrication, and Wear Technology. pg 266-289. 2017.

Zhuk, Y. *Nano-Structured CVD Tungsten Carbide Coating Protects Against Wear and Corrosion*. Hardide Plc. 2010.

9. Appendix

A. Stellite alloy compositions and properties

Alloy	COMP	Hardness H.R.C.	Melting Range °C	Typical Applications
Stellite™ 1	C 2.5 Cr 32 W 13 Co Bal	55	1250-1290	Very high resistance to abrasion and corrosion. Retains hardness at temperatures in excess of 600°C. Used for pump sleeves, rotary seal rings, wear pads, bearing sleeves, extruder screw flights. Also available as rod, wire and electrode.
Stellite™ 6	C 1 Cr 27 W 5 Co Bal	42	1280 - 1390	Tough erosion-resistant alloy widely used for good all round performance. Less tendency to crack than Stellite™ 12 in multiple layer, but more wear resistant than Stellite™ 21 in abrasion and metal to metal conditions. Good impact conditions. Good impact resistance. Valve seats and gates; pump shafts and bearings, erosion shields and rolling couples. Often used self-mated. Can be turned with carbide tooling. Also available as rod, electrode and wire.
Stellite™ 7	C 0.4 Cr 26 W 5.5 Co Bal	35	1300 - 1390	Similar to Stellite™ 6 but with lower hardness, this alloy contains fewer hard carbides. This feature ensures very high corrosion and erosion resistance. Has high impact resistance. Also available as rod and wire.
Stellite™ 12	C 1.8 Cr 30 W 9 Co Bal	48	1280 - 1315	Properties between those of Stellite™ 1 and Stellite™ 6. More abrasion resistance than Stellite™ 6, but still good impact resistance. Widely used as cutting edge in textile, timber and plastics industries and for bearings. Also available as rod, electrode and wire.
Stellite™ 20	C 2.5 Cr 32 W 17 Co Bal	58	1260 - 1320	The most abrasion resistant standard cobalt base alloy. While it has low shock resistance it is often the only answer for some applications, such as slurry pumps or chemical resistant parts. Also available by rod and electrode. Finish by grinding only.
Stellite™ 21	C 0.2 Cr 27 Mo 5 Co Bal	32	1180 - 1380	Excellent resistance to thermal and mechanical shock. Excellent high temperature strength. Applications involving erosion, high temperatures and corrosion. Valve trim for high pressure steam, oil and petrochemical. Also available as rod, electrode and wire.
Stellite™ 31	C 0.5 Cr 26 W 7 Co Bal Ni 10	32	1260 - 1415	Excellent high temperature strength and oxidation resistance. Excellent resistance to thermal and mechanical shock. Mainly used in gas turbine engines in areas subject to hot gas erosion. Conforms to PWA:1318/DMR 33.007/ MIL-P-83348-1-C12 Also available as rod. Approved to MSRR 9707/3
Stellite™ 157	Cr 22 W 4.5 Co Bal B 2.4	52	1070 - 1110	An alloy similar to Stellite™ SF1 and often used as an alternative for bearings, rollers, and wear rings. Modified fusing characteristics make this a favorite alloy for many users. Spray fuse coating of Stellite™ 157 can be applied quickly and easily with the minimum of equipment. Powder weld deposits may be applied to small or large areas with ease. Useful for edge build up.
Stellite™ 306	Cr 25 W 2 Co Bal Ni 6 Nb 5 Fe 4 C 0.4	35	1260 - 1310	Similar properties to Stellite™ 6, but slightly softer to improve resistance to thermal and mechanical shock. Mainly used on large, heavy restrained components such as roll and marine bearings where it would be difficult to avoid stress cracking during hard facing with Stellite™ 6. Also available as rod, electrode and wire.
Stellite™ 694	C 1 Cr 28 W 19 Co Bal Ni 5 V 1	50	1280 - 1360	High strength cobalt base super alloy with fine micro-structural characteristics and high temperature stability. Resistant to erosion, cavitation and fine particle abrasion. Used in gas turbine parts where a higher hardness than Stellite™ 31 is required. Also available as rod.
Stellite™ F	C 1.7 Cr 25 W 12 Co Bal Ni 22	44	1260 - 1305	Slightly higher hardness and fluidity than Stellite™ 6. Good erosion and corrosion resistance. Used primarily for deposition on closing face of poppet valves for internal combustion engines. Also available as rod.

B. Raw Erosion Data

Table BI - Raw Mass Loss and Time Data of Conforma Clad WC210 at 95 psi:

WC210						
Trail #	Sample #	Initial Mass (g)	Erosion Mass (g)	Mass Loss (g)	Mass Loss (mg)	Time (s)
Trail #1	WC210-1-1	102.7569	102.3821	0.3748	374.8000	60.45
	WC210-1-2	120.1804	119.4332	0.7472	747.2000	120.27
	WC210-1-3	119.0058	117.9413	1.0645	1064.5000	180.36
	WC210-1-4	122.7547	121.2922	1.4625	1462.5000	240.42
Trial #2	WC210-2-1	126.3576	126.0266	0.3310	331.0000	60.42
	WC210-2-2	123.6014	122.9623	0.6391	639.1000	120.34
	WC210-2-3	120.7994	119.8302	0.9692	969.2000	180.4
	WC210-2-4	119.0671	117.7381	1.3290	1329.0000	240.45
Trial #3	WC210-3-1	125.5811	125.2395	0.3416	341.6000	60.72
	WC210-3-2	123.0542	122.4159	0.6383	638.3000	120.4
	WC210-3-3	125.1038	124.1393	0.9645	964.5000	180.48
	WC210-3-4	124.5034	123.2438	1.2596	1259.6000	240.53

Table B2 - Raw Mass Loss and Time Data of Conforma Clad WC219 at 95 psi:

WC219						
Trail #	Sample #	Initial Mass (g)	Erosion Mass (g)	Mass Loss (g)	Mass Loss (mg)	Time (s)
Trail #1	WC219-1-1	127.3564	126.6779	0.6785	678.5	120.32
	WC219-1-2	128.7550	128.3605	0.3945	394.5	60.36
	WC219-1-3	128.9455	127.8743	1.0712	1071.2	180.51
	WC219-1-4	106.1858	104.7507	1.4351	1435.1	240.58
Trial #2	WC219-2-1	123.1862	122.8193	0.3669	366.9	60.39
	WC219-2-2	125.4680	124.7602	0.7078	707.8	120.44
	WC219-2-3	128.4056	127.3769	1.0287	1028.7	180.41
	WC219-2-4	128.7721	127.4898	1.2823	1282.3	240.41
Trial #3	WC219-3-1	122.2373	121.5877	0.6496	649.6	120.52
	WC219-3-2	121.1545	119.7169	1.4376	1437.6	240
	WC219-3-3	121.2202	120.4444	0.7758	775.8	60
	WC219-3-4	121.5684	120.4472	1.1212	1121.2	180.32

Table B3 - Raw Mass Loss and Time Data of Conforma Clad A36 Steel at 95 psi:

A36						
Trail #	Sample #	Initial Mass (g)	Erosion Mass (g)	Mass Loss (g)	Mass Loss (mg)	Time (s)
Trial #1	S-1-1	93.7825	93.6437	0.1388	138.8	60.38
	S-1-2	98.1734	97.8928	0.2806	280.6	120.33
	S-1-3	91.2958	90.8588	0.437	437	180.39
	S-1-4	86.0621	85.4774	0.5847	584.7	240.67
Trial #2	S-2-1	93.4640	93.3233	0.1407	140.7	60.47
	S-2-2	93.7275	93.4488	0.2787	278.7	120.41
	S-2-3	97.9080	97.4882	0.4198	419.8	180.42
	S-2-4	90.2228	89.669	0.5538	553.8	240.43
Trial #3	S-3-1	93.1892	92.9145	0.2747	274.7	120.55
	S-3-2	92.1330	91.9946	0.1384	138.4	60.43
	S-3-3	87.5799	87.1642	0.4157	415.7	180.42
	S-3-4	88.8267	88.2869	0.5398	539.8	240.45

Table B4 - Raw Mass Loss and Time Data of Conforma Clad Hardide-T at 95 psi:

Hardide-T						
Trail #	Sample #	Initial Mass (g)	Erosion Mass (g)	Mass Loss (g)	Mass Loss (mg)	Time (s)
Trial #1	H-1-1	103.6121	103.4559	0.1562	156.2	N/A
	H-1-2	107.9724	107.6673	0.3051	305.1	N/A
	H-1-3	104.1605	103.7235	0.437	437	N/A
	H-1-4	103.0426	102.4812	0.5614	561.4	N/A
Trial #2	H-2-1	108.087	108.0569	0.0301	30.1	105
	H-2-2	110.3349	110.2374	0.0975	97.5	210
	H2-3	103.8511	103.7111	0.14	140	315
	H-2-4	104.1487	103.9477	0.201	201	420
Trial #3	H-3-1	104.9761	N/A	104.9761	104976.1	N/A
	H-3-2	74.1537	N/A	74.1537	74153.7	N/A
	H-3-3	102.6805	N/A	102.6805	102680.5	
	H-3-4	107.9076	N/A	107.9076	107907.6	N/A

Table B5 - Raw Mass Loss and Time Data of Conforma Clad WC210 at 40 psi:

WC210						
Trail #	Sample #	Initial Mass (g)	Erosion Mass (g)	Mass Loss (g)	Mass Loss (mg)	Time (s)
Trial #1	WC210-2-3	119.8302	119.8078	0.0224	22.4000	105
	WC210-1-2	119.4332	119.3561	0.0771	77.1000	210
	WC210-2-2	122.9623	122.8388	0.1235	123.5000	315
	WC210-3-1	125.2395	125.0741	0.1654	165.4000	420
Trial #2	WC210-3-4	123.2438	123.2208	0.0230	23.0000	105
	WC210-3-3	124.1393	124.0825	0.0568	56.8000	210
	WC210-3-2	122.4159	122.3261	0.0898	89.8000	315
	WC210-2-1	126.0266	125.8955	0.1311	131.1000	420

Table B6 - Raw Mass Loss and Time Data of Conforma Clad A36 Steel at 40 psi:

A36						
Trail #	Sample #	Initial Mass (g)	Erosion Mass (g)	Mass Loss (g)	Mass Loss (mg)	Time (s)
Trial #1	S-2-1	93.3233	93.2675	0.0558	55.8	105
	S-2-2	93.4488	93.3235	0.1253	125.3	210
	S-2-3	97.4882	97.2862	0.202	202	315
	S-1-1	93.6437	93.361	0.2827	282.7	420
Trial #2	S-3-1	92.9145	92.865	0.0495	49.5	105
	S-3-2	91.9946	91.8775	0.1171	117.1	210
	S-3-3	87.1642	86.9759	0.1883	188.3	315
	S-1-2	97.8928	97.6374	0.2554	255.4	420

Table B7 - Raw Mass Loss and Time Data of Conforma Clad Hardide-T at 40 psi:

Hardide-T						
Trail #	Sample #	Initial Mass (g)	Erosion Mass (g)	Mass Loss (g)	Mass Loss (mg)	Time (s)
Trial #1	H-2-1	108.087	108.0569	0.0301	30.1	105
	H-2-2	110.3349	110.2374	0.0975	97.5	210
	H2-3	103.8511	103.7111	0.14	140	315
	H-2-4	104.1487	103.9477	0.201	201	420
Trial #2	H-3-1	104.9761	104.9438	0.0323	32.3	105
	H-3-2	74.1537	74.0599	0.0938	93.8	210
	H-3-3	102.6805	102.5558	0.1247	124.7	315
	H-3-4	107.9076	107.7173	0.1903	190.3	420

C. Raw Hardness Data

Table C1 - WC219 & WC210 Rockwell Hardness HRC Raw Data:

Hardness (HRC)									
WC 219			WC 219 (eroded)		WC 210			WC 210 (eroded)	
Sample 1-1	Sample 3-4	Sample 2-3	Sample 2-3	Sample 3-4	Sample 2-4	Sample 3-1	Sample 1-2	Sample 2-4	Sample 3-1
50.1	57.0	54.5	53.9	37.9	45	62.8	59.6	44.6	50.6
59.7	57.0	54.1	54.5	53.8	56.7	64.3	57.7	51.9	59.3
53.5	55.4	56.3	45	51	57.7	64.1	59.3	58.4	56.6
56.6	56.4	56.5	8.4	56.7	57.7	63.7	58.6	57.2	56.9
Average	55.59		Average	45.15	Average	58.93		Average	54.44
Standard Deviation	2.37		Standard Deviation	16.08	Standard Deviation	5.20		Standard Deviation	5.01

Table C2 - A36 Steel and Hardide-T Rockwell Hardness HRB Raw Data:

Hardness (HRB)						
A36 Steel			A36 Steel (eroded)		Hardide-T	
Sample 3-4	Sample 1-3	Sample 2-2	Sample 3-4	Sample 1-3	H	H-1
71	75	71	66.7	73.3	84.8	81.1
71.1	74.6	70.1	67.7	72.6	84.1	81.4
72.2	75.2	68.1	69.1	73.4	83.3	81.4
71.9	74.8	71.7	69.4	72.2	84.2	82.2
Average	72.23		Average	70.55	Average	82.8125
Standard Deviation	2.24		Standard Deviation	2.65	Standard Deviation	1.46